

Finite difference method for the acoustic radiation of an elastic plate excited by a turbulent boundary layer: a spectral domain solution

Daniel Mazzoni, U. Kristiansen

▶ **To cite this version:**

Daniel Mazzoni, U. Kristiansen. Finite difference method for the acoustic radiation of an elastic plate excited by a turbulent boundary layer: a spectral domain solution. Flow, Turbulence and Combustion, 1998, 61 (1-4), pp.133-159. 10.1023/A:1026440919022 . hal-01004490

HAL Id: hal-01004490
https://hal.science/hal-01004490

Submitted on 11 Jun 2014

HAL is a multi-disciplinary open access archive for the deposit and dissemination of scientific research documents, whether they are published or not. The documents may come from teaching and research institutions in France or abroad, or from public or private research centers.

L'archive ouverte pluridisciplinaire **HAL**, est destinée au dépôt et à la diffusion de documents scientifiques de niveau recherche, publiés ou non, émanant des établissements d'enseignement et de recherche français ou étrangers, des laboratoires publics ou privés.

Finite Difference Method for the Acoustic Radiation of an Elastic Plate Excited by a Turbulent Boundary layer : A Spectral Domain Solution

Daniel Mazzoni
Laboratoire de Mécanique et d'Acoustique - ESM2
31 chemin Joseph-Aiguier
13402 Marseille cedex 20 (France)
Tel : (0) 491 05 46 16 Fax : (0) 491 05 45 98
e-mail : mazzoni@esm2.imt-mrs.fr

Ulf Kristiansen
Norwegian Institute of Science and Technology
Acoustics Group
7034 Trondheim (Norway)
Tel : +47 7359 26 34 Fax : +47 7359 14 128
e-mail Kristian@tele.ntnu.no

september 1997

Abstract

A finite difference method is developed to study, on a 2D model, the acoustic pressure radiated when a thin elastic plate, clamped at its boundaries, is excited by a turbulent boundary layer.
Consider an homogeneous thin elastic plate clamped at its boundaries and extended to infinity by a plane, perfectly rigid, baffle. This plate closes a rectangular cavity. Both the cavity and the outside domain contain a perfect fluid. The fluid in the cavity is at rest. The fluid in the outside domain moves in the direction parallel to the system plate/baffle with a constant speed. A turbulent boundary layer developes at the interface baffle/plate. The wall pressure fluctuations in this boundary layer generates a vibration of the plate and an acoustic radiation in the two fluid domains.
Modeling the wall pressure fluctuations spectrum in a turbulent boundary layer developed over a vibrating surface is a very complex and unresolved task. Ducan and Sirkis [1] propose a model for the two-way interactions between a membrane and a turbulent flow of fluid. The excitation of the membrane is modeled by a potential flow randomly perturbed. This potential flow is modified by de displacement of the membrane. Howe [2] proposes a model for the turbulent wall pressure fluctuations power spectrum over an elastomeric material. The model presented in this article is based on an hypothesis of one-way

interaction between the flow and the structure: The flow generates wall pressure fluctuations which are at the origin of the vibration of the plate, but the vibration of the plate does not modify the characteristics of the flow.
A finite difference scheme that incorporates the vibration of the plate and the acoustic pressure inside the fluid cavity has been developed and coupled with a boundary element method that ensures the outside domain coupling. In this paper, we focus on the resolution of the coupled vibration/interior acoustic problem. We compare the results obtained with three numerical methods: (a) A finite difference representation for both the plate displacement and the acoustic pressure inside the cavity. (b) A coupled method involving a finite difference representation for the displacement of the plate and a boundary element method for the interior acoustic pressure. (c) A boundary element method for both the vibration of the plate and the interior acoustic pressure.
A comparison of the numerical results obtained with two models of turbulent wall pressure fluctuations spectrums, the Corcos model [3] and the Chase model [4], is proposed. A difference of 20dB is found on the vibro-acoustic response of the structure. In [5] this difference is explained by calculating a wavenumber transfer function of the plate. In [6], coupled beam-cavity modes for similar geometry are calculated by the finite difference method.

1 Introduction

The calculation of the flow induced sound and vibrations has been the focus of considerable work. The development of high-speed transport is certainly at the origin of this interest. As the flow induced sound become a non negligible part of the noise into a car or a plane, there is an important economic interest in reducing this noise. This reduction involves the knowledge of the mechanisms by witch a turbulent boundary layer induces a vibration of a structure.

In the 2 dimensional domain R^2, consider a Cartesian set of coordinates $(0, \mathbf{x}, \mathbf{z})$. A thin elastic one-dimensional plate Σ of length L and thickness $e << L$ occupies the open domain $\{M(x,z)/0 < x < L, -e/2 \leq z \leq e/2\}$. This plate encloses a rectangular cavity of height H and length L. For simplicity, we assume that the plate is homogeneous and isotropic and we model its motion by using the Kirchhoff-Helmholtz theory. Then, the one-dimensional plate Σ reduces to a line $\Sigma = \{M(x,0)/0 < x < L\}$ and its mechanical properties are: A bending stiffness $D = Eh^3/(12(1-\nu^2))$ and a mass per unit area μ, where E and ν are the Young modulus and the Poisson ratio of the material. Let us denote $\partial\Sigma = \{0, L\}$ the boundaries of this plate and $\overline{\Sigma}$ the enclosure of Σ. A perfectly rigid baffle occupies the domain $\{M(x,z)/z = 0\} - \overline{\Sigma}$.

The domain $z < 0$ contains a rectangular cavity surrounded by 3 walls denoted σ and by the plate Σ. We denote Ω_e the exterior domain ($z > 0$) and Ω_i the fluid cavity. Both the domains Ω_e and Ω_i contain a perfect fluid characterized by a density ρ_e and ρ_i and sound speeds c_e and c_i. The fluid in the exterior domain is moving in the direction parallel to the plate with the constant speed u_∞. A turbulent boundary layer developes at the interface between the fluid and the system plate/baffle. The wall pressure fluctuations in this turbulent boundary layer induce a vibration of the plate and a noise in the two fluid domains. For simplicity, we make the two following assumptions: (a) In the turbulent boundary layer, the wall pressure fluctuations are

not modified by the vibration of the plate. (b) For the acoustic propagation in Ω_e, we consider that the fluid is at rest.

One of the first model for the vibro-acoustic response of a rectangular plane panel excited by a turbulent boundary layer is du to Davies [7]. The author considers a simply-supported plate immersed in air and performs a modal approach and a light-fluid approximation to calculate the displacement of the plate. Recently, a more complete investigation of this modal approach is proposed by Robert [8]. In both these models, the turbulent excitation is given under the form of a space-frequency spectrum. In the present article, the suitability of a wavenumber-frequency ($\mathbf{k}$-ϵ) spectrum for predicting the vibro-acouctic response of an elastic structure excited by a turbulent boundary layer is investigated through a simple 2D model.

2 Green's representations of the displacement and of the acoustic pressure

In this paragraph, we establish the Green's representations of the displacement of the plate and of the acoustic pressure field in Ω_e and Ω_i. For simplicity, we consider the case of a clamped beam coupled to a semi-infinite fluid domain Ω_e and excited by an harmonic force $f(x)e^{-\imath\omega t}$ acting in the direction parallel to the z-axis. The displacement $u(x)$ and the acoustic pressure $p_e(\mathbf{M})$ in Ω_e are solution of the following system of differential equations:

$$\begin{cases} D\dfrac{\partial^4}{\partial x^4}u(x) - \mu\omega^2 u(x) = -f(x) - p_e(x,0), \quad \forall x \in \Sigma \\ \Delta p_e(x,z) + k_e^2 p_e(x,z) = 0, \quad \forall (x,z) \in \Omega_e \\ u(x) = u'(x) = 0, \quad \forall x \in \partial\Sigma \\ \dfrac{\partial p_e}{\partial z}(x,0) = \rho_e\omega^2 u(x), \quad \forall x \in \Sigma \\ \dfrac{\partial p_e}{\partial z}(x,0) = 0, \quad \forall x \in \text{baffle} \\ \text{Sommerfeld radiation conditions.} \end{cases} \tag{1}$$

In this system, Δ is the Laplacian calculated with respect the variables x and z, k_e denotes the acoustic wavenumber in the exterior domain ($k_e = \omega/c_e$), ω is the angular frequency.

The Green's representation of the acoustic pressure in the semi-infinite domain Ω_e is given by the following integral:

$$p_e(x,z) = -\frac{\imath\omega^2\rho_e}{2}\int_0^L H_0\left(k_e\sqrt{(x-x')^2+z^2}\right)\, u(x')\, dx' \tag{2}$$

The Green's kernel Γ of the displacement of the fluid-loaded baffled plate is cal-

culated by introducing the Green's representation (2) into the system (1):

$$\begin{cases} D\dfrac{\partial^4}{\partial x^4}\Gamma(x) - \mu\omega^2\Gamma(x) - \dfrac{\imath\omega^2\rho_e}{2}\displaystyle\int_0^L H_0\left(k_e|x-x'|\right)\ \Gamma(x')\ dx' = -\delta(x), \quad \forall x \in \Sigma \\ \Gamma(x) = \Gamma'(x) = 0, \quad \forall x \in \partial\Sigma \\ \Gamma(x) = 0, \quad \forall x \in \text{baffle} \end{cases} \tag{3}$$

The kernel Γ gives access to an expression for the displacement u of the fluid-loaded baffled plate excited by the harmonic force of amplitude f. The displacement u, which is solution of the system (1), takes the form of a convolution product between the kernel Γ and the force f:

$$\begin{aligned} u(x) &= \int_0^L \Gamma(x')\ f(x-x')\ dx' \ = \ \Gamma * f, \quad \forall x \in \Sigma \\ &= 0, \quad \forall x \in \text{baffle} \end{aligned} \tag{4}$$

The acoustic pressure field in the exterior domain is calculated by introducing the displacement (4) in the Green's representation (2).

This formalism extends to the problem of a plate coupled with both a semi-infinite fluid domain and a fluid cavity. The acoustic pressure inside the cavity is then calculated by the Green's representation presented in [9].

3 Response of the plate to a space and time random excitation

The excitation force f modeling the wall pressure fluctuations in a turbulent boundary layer is a random field stationary up to order 2 with respect to the space and time variables. The autocorrelation function R_f of the turbulent excitation f is defined as follows:

$$R_f(x,t) = \mathbf{E}\left[f(x',t')\ f^*(x'-x,t'-t)\right] \tag{5}$$

where z^* denotes the conjugate of the complexe number z.

The function R_f possesses a 2D Fourier transform, denoted S_f, with respect to the space coordinate x and the time variable t. This Fourier transform S_f is the wavenumber-frequency power spectrum of the excitation force f:

$$S_f(k_x,\omega) = \int_{-\infty}^{\infty}\int_{-\infty}^{\infty} R_f(x,t)\ e^{\imath(\omega t - k_x x)}\ dx\ dt \tag{6}$$

In formula (6), k_x is the wavenumber in the direction x. This paper deals with the comparison of the results obtained, in terms of the vibro-acoustic response of an elastic panel, when the turbulent excitation is given by two different models of wall pressure wavenumber-frequency power spectrum: The Corcos model [3] and the Chase model [4].

The cross correlation function of the displacement R_u of the fluid-loaded plate is stationary up to order 2 with respect to the time but not stationary with respect to the space coordinate x. This function R_u is defined as follows:

$$R_u(x,x',t) = \mathbf{E}\left[u(x,t')\ u^*(x',t'-t)\right] \tag{7}$$

where x and x' denote two points on the plate Σ. Introducing the expression (4) of the displacement in the formula (7) leads to an integral representation of the cross correlation function R_u:

$$R_u(x,y,t) = \int_{-\infty}^{\infty}\int_{-\infty}^{\infty}\int_0^L\int_0^L \gamma(x-x',t-t') \\ R_f(x'-y',t'-\tau')\ \gamma^*(y-y',\tau-\tau')\ dx'\,dy'\,dt'\,d\tau' \tag{8}$$

The function R_u possesses a time Fourier transform because both the Green's kernel γ and the autocorrelation function R_f possess a time Fourier transform. Performing the time Fourier transform of the formula (8) leads to an expression of the frequency cross spectrum of the displacement of the plate:

$$S_u(x,y,\omega) = \int_0^L\int_0^L \Gamma(x-x',\omega)\ S_f^T(x'-y',\omega)\ \Gamma^*(y-y',\omega)\ dx'\ dy' \tag{9}$$

The function Γ which appears in the integral (9) is the time Fourier transform of the Green's kernel γ. The function S_f^T is the frequency power spectrum of the random excitation f. It is a power spectrum calculated with respect the time variable. The expression (9) of the frequency cross spectrum is used by Robert [8] and Bano & al. [10] to calculate the vibro-acoustic response of a panel excited by a turbulent flow of fluid.

Recently, Chase [11] [4] [12] proposes a model for the wall pressure fluctuations wavenumber-frequency power spectrum in turbulence. The Chase model consists in an analytical expression of the wavenumber-frequency power spectrum presented in the formula (6). It is valid for a turbulent flow of fluid at low Mach number. The Chase model is not a frequency power spectrum as used in the integral (9). When the turbulent excitation is given by the Chase model, it is clear that the response of the plate can be calculated by performing an inverse Fourier transform of the expression (6) with respect the wavenumber k_x and by introducing this inverse Fourier transform in the integral (9). But this is a great deal of computational power. A few considerations can reduce this large amounts of calculus. The frequency power spectrum S_f^T is the inverse space Fourier transform of the wavenumber-frequency power spectrum S_f defined by the formula (6):

$$S_f^T(x-y,\omega) = \frac{1}{2\pi}\int_{-\infty}^{\infty} S_f(k_x,\omega)\ e^{\imath k_x(x-y)}\ dk_x \tag{10}$$

The formula (10), introduced in the expression (9), leads to:

$$S_u(x,y,\omega) = \int_{-\infty}^{\infty} U(x,k_x,\omega)\ S_f(k_x,\omega)\ U^*(y,k_x,\omega)\ dk_x \tag{11}$$

where $U(x,k_x,\omega)$ is the displacement of the plate, calculated at the angular frequency ω, when the excitation force f reduces to the contribution of one wavenumber k_x. The function $U(x,k_x,\omega)$ is calculated by solving the system (1) for an excitation force f taken equal to $e^{\imath k_x x}$.

The frequency cross spectrum of the acoustic pressure at the points M and M' in Ω_e expresses in the same way:

$$S_{p_e}(M,M',\omega) = \int_{-\infty}^{\infty} P_e(M,k_x,\omega)\ S_f(k_x,\omega)\ P_e^*(M',k_x,\omega)\ dk_x \tag{12}$$

where $P_e(M, k_x, \omega)$ is the solution p_e of the system (1) calculated when $f(x) = e^{\imath k_x x}$.

The expression (11) of the frequency cross spectrum is equivalent to the expression (9). However, the formula (11) is more interesting that the formula (9). The first advantage concerns the physical interpretation of the results. The function:

$$k_x \longrightarrow U(x, k_x, \omega)\ S_f(k_x, \omega)\ U^*(x, k_x, \omega) \tag{13}$$

defines an instantaneous spectral density function [13]. This function represents the response of the plate at the point x to one wavenumber k_x. The function:

$$k_x \longrightarrow U(x, k_x, \omega)\ U^*(x, k_x, \omega) \tag{14}$$

is a transfer function. It is a measure of the wavenumber filtering of the plate at the point x. The functions (13) and (14) permit to represent the plate as a wavenumber filter. The second advantage of the formula (11) is a numerical one: The formula (9) imposes to perform a double integration of a function whose oscillations increase when the difference $x' - y'$ tends to zero. Using the formula (9), the cross spectrum S_u is given by calculating a simple infinite integral of an oscillating function of constant period. Moreover, this instantaneous spectral density function is maximum in at the origin ($k_x = 0$) (or in a region very close to the origin) and decreases very quickly as the wavenumber $|k_x|$ increases. So, the integral (11) can be calculated with a good accuracy by using a simple constant step integration pattern. In this paper, we use a Gauss integration scheme.

4 Governing system of equations

The vibro-acoustic response of a 1D-plate coupled with a fluid cavity and with an infinite fluid domain to a turbulent boundary layer is expressed by using the instantaneous spectral density function presented in the precedent paragraph. The cross spectral density functions of the displacement of the plate and of the acoustic pressure in the exterior domain are given by the formulas (11) and (12). The cross spectral density function of the acoustic pressure inside the cavity is given by the following integral:

$$S_{p_i}(M, M', \omega) = \int_{-\infty}^{\infty} P_i(M, k_x, \omega)\ S_f(k_x, \omega)\ P_i^*(M', k_x, \omega)\ dk_x \tag{15}$$

where $S_f(k_x, \omega)$ is the wavenumber-frequency power spectrum of the wall pressure fluctuations in the turbulent boundary layer. The functions $U(x, k_x, \omega)$, $P_e(M, k_x, \omega)$ and $P_i(M, k_x, \omega)$ are the responses of the physical system to the determinist excitation $e^{\imath k_x x}$. These functions $U(x, k_x, \omega)$, $P_e(M, k_x, \omega)$ and $P_i(M, k_x, \omega)$ are the solutions of

the following system of differential equations:

$$
\begin{aligned}
D\frac{\partial^4}{\partial x^4}U(x,k_x,\omega) - \mu\omega^2 U(x,k_x,\omega) &= -e^{\imath k_x x} \\
-P_e(M,k_x,\omega) + P_i(M,k_x,\omega), \quad \forall M(x,0) \in \Sigma & \qquad (a) \\
U(x,k_x,\omega) = \partial_x U(x,k_x,\omega) = 0, \quad \forall x \in \partial\Sigma & \qquad (b) \\
\Delta P_e(M,k_x,\omega) + k_e^2 P_e(M,k_x,\omega) = 0, \quad \forall M(x,z) \in \Omega_e & \qquad (c) \\
\frac{\partial P_e}{\partial z}(M,k_x,\omega) = \rho_e\omega^2 U(x,k_x,\omega), \quad \forall M(x,0) \in \Sigma & \qquad (d) \\
\frac{\partial P_e}{\partial z}(M,k_x,\omega) = 0, \quad \forall M(x,0) \in \text{baffle} & \qquad (e) \\
\Delta P_i(M,k_x,\omega) + k_i^2 P_i(M,k_x,\omega) = 0, \quad \forall M(x,z) \in \Omega_i & \qquad (f) \\
\frac{\partial P_i}{\partial z}(M,k_x,\omega) = \rho_i\omega^2 U(x,k_x,\omega), \quad \forall M(x,0) \in \Sigma & \qquad (g) \\
P_i(M,k_x,\omega) = 0, \quad \forall M \in \sigma & \qquad (h) \\
\text{Sommerfeld radiation conditions.}
\end{aligned}
\tag{16}
$$

where k_i denotes the acoustic wavenumber inside the cavity ($k_i = \omega/c_i$).

As a prelude to this study, a few comments are appropriate concerning the physics of the problem. The experience pointed out that the vibro-acoustic response of a steel plate coupled with an infinite fluid domain is mainly governed by the vibrations of the structure. The influence of the fluid reduces to a perturbation of the vibratory response of the plate. This perturbation can be large if we consider the case of a plate coupled to a heavy fluid, and small in the case of coupling to a light fluid. Concerning the acoustic coupling between a plate and a fluid cavity with rigid walls, it should be mentioned that for very shallow cavities, the stiffness of even light fluids might be comparable to the stiffness of the elastic structure.
As a consequence of these comments, in this paper, we analyse the relative performances of high-order finite-difference schemes applied to the resolution of the *in vaccuo* plate equation, and we compare the numerical results otained with two different methods for the interior domain acoustic coupling of this plate: A boundary element method and a finite difference method.

5 Finite difference scheme for solving the plate equation

A pragmatic approach has been used to investigate the relative performances of high-order finite difference schemes applied to the computation of a plate equation. We compute the solutions of an *in vaccuo* clamped plate on a fixed grid of N points $x_j = j\Delta x$ ($j = 0, 1, .., N-1$), with central finite difference schemes of the following orders of accuracy: $O(\Delta x^2)$, $O(\Delta x^4)$, $O(\Delta x^6)$ and $O(\Delta x^{12})$.

The equation of the displacement of an *in vaccuo* clamped plate excited by a point harmonic force, applied at the abscisse Δx, in the direction parallel to the

z-coordinate, is:

$$\begin{cases} \dfrac{\partial^4}{\partial x^4} u(x) - \mu\omega^2 u(x) = \delta(x - \Delta x) \\ u(x_0) = u(x_{N-1}) = u'(x_0) = u'(x_{N-1}) = 0 \end{cases} \tag{17}$$

where $u(x)$ is the normal displacement of the plate at the point x and where $\delta(x-\Delta x)$ is the Dirac delta function at the point Δx.

The central finite difference schemes of orders 2, 4, 6 and 12 approximating the fourth-order derivative operator are presented in the appendix A. A study of the truncation error analysis is presented, as an example, for the second order finite difference scheme, in the appendix B.
For simplicity, the finite difference solution of the equation (17) is written for the case of the use of an order 2 central difference scheme. The use of an upper order differencing scheme brings more equations but no more theoretical difficulty.
The second order finite difference discretization of the equation (17) leads to a linear system composed of $N-2$ algebraic equations and $N-2$ unknowns. This system consists in $N-6$ equations for the displacement u_j of the plate at the points x_j (apart from the boundary conditions):

$$\frac{D}{\Delta x^4}\{u_{j-2} - 4u_{j-1} + 6u_j - 4u_{j+1} + u_{j+2}\} - \mu\omega^2 u_j = \delta(x_j - \Delta x) \;\; 3 \leq j \leq N-4 \tag{18}$$

Four equations must be added to takes into account the boundary conditions. For a clamped plate, these equations are obtained by "folding away" the differencing scheme with respect the bounds of the plate:

$$\begin{aligned}
j = 1 \qquad & u(x=0) = 0 \Rightarrow u_0 = 0 \\
& \frac{\partial u}{\partial x}(x=0) = 0 \Rightarrow u_{-1} = u_1 \\
& \Rightarrow \frac{D}{\Delta x^4}\{7u_1 - 4u_2 + u_3\} - \mu\omega^2 u_1 = 1 \\
j = 2 \qquad & u(x=0) = 0 \Rightarrow u_0 = 0 \\
& \Rightarrow \frac{D}{\Delta x^4}\{-4u_1 + 6u_2 - 4u_3 + u_4\} - \mu\omega^2 u_2 = 0 \\
j = N-3 \quad & u(x=L) = 0 \Rightarrow u_{N-1} = 0 \\
& \Rightarrow \frac{D}{\Delta x^4}\{u_{N-5} - 4u_{N-4} + 6u_{N-3} - 4u_{N-2}\} - \mu\omega^2 u_{N-3} = 0 \\
j = N-2 \quad & u(x=L) = 0 \Rightarrow u_{N-1} = 0 \\
& \frac{\partial u}{\partial x}(x=L) = 0 \Rightarrow u_N = u_{N-2} \\
& \Rightarrow \frac{D}{\Delta x^4}\{u_{N-4} - 4u_{N-3} + 7u_{N-2}\} - \mu\omega^2 u_{N-2} = 0
\end{aligned} \tag{19}$$

The second order finite difference solution of the *in vaccuo* clamped plate equation (17) consists in solving a linear system composed of the algebraic equations (18, 19).

Because of the practical constraints inherent in the memory implementation of large-scale computing methods, the judgement of the efficiency of a finite difference scheme must consider both the memory demands and the precision of the algorithm.

Solving the *in vaccuo* plate equation (17) by performing a n^{th}-order accurate central finite difference method on a N points grid requires to inverse a $N \times N$ matrix which contains $N(n+3) - (n+4)(n+6)/4$ non-zero real floating-point elements. The accuracy of the solution is then $O(\Delta x^n)$. The interest of an high-order method is then evident in terms of memory saving. The major restriction to the use of an high-order finite difference scheme lies in the fact that the numerical dispersion increases when performing an oversampling (in terms of points per elastic wavelength) of the structure.

A pragmatic approach is proposed to investigate the numerical dispersion of the central finite difference schemes of orders 2, 4, 6 and 12 presented in the appendix A. A representative test case as been computed. It consists in the numerical calculation of the first resonance frequencies of an *in vaccuo* steel beam, clamped at its boundaries. These resonance frequencies arise from the calculation of the local minimums of the spectrum of the determinant of the linear set of algebraic equations outcoming from the finite difference discretization of the system (17). For the case of a second-order finite difference solution, it is the determinant of the system composed of the equations (18, 19). These eigenfrequencies are compared to the natural frequencies of a clamped *in vaccuo* beam calculated in an analytical way by Leissa [14]. The spectrum of the determinant has been computed with a frequency step equal to $0.1\,Hz$. The mechanical properties of the structure for this test-case are the following:

Length :	$L = 1\,m$
Thickness :	$e = 0.004\,m$
Young's modulus :	$E = 210^{11}\,Nm$
Poisson ratio :	$\nu = 0.3$
Mass per unit area	$\mu = 7800 \cdot e\ Kgm^{-2}$
Mesh-grid :	$N = 51$ points

The results of this numerical study are presented in the following table:

Table 1. Numerical dispersion of order 2, 4, 6, 12 finite difference schemes

mode	sampling rate (points per wavelength)	resonance frequencies Hz				
		analytical calculation	finite difference			
			order 2	ordre 4	order 6	ordre 12
1	51	21.7	21.7	21.7	21.7	21.8
2	26	60.1	59.8	60.1	60.1	60.2
3	17	117.8	117.1	117.8	117.8	118
4	13	194.9	193	194.8	194.9	195
5	10	291.1	287.3	291	291.1	291.2
6	8	406.7	399.5	406.3	406.6	406.7
7	7	541.5	529.1	540.7	541.4	541.5
8	6	695.5	675.7	694.1	695.3	695.5
9	6	868.8	838.6	866.3	868.5	868.8
10	5	1061.4	1017.2	1057.1	1060.8	1061.4
11	5	1273.2	1210.7	1266.3	1272.2	1273.2
12	4	1504.3	1418.5	1493.6	1502.6	1504.3
13	4	1754.6	1639.5	1738.6	1751.8	1754.6

The comparisons presented in the Table 1 point out that the second and fourth-order finite difference schemes requires an heavy oversampling of the model to give an accuracy of the order of $0.1\,Hz$. More than 20 points per wavelength are required for the second-order scheme and approximatly 10 points per wavelength for the fourth-order scheme. The sixth-order finite difference scheme gives a good accuracy with a sampling rate equal to 7 points per wavelength. The finite difference scheme of order 12 gives the exact values (with an accuracy of $0.1\,Hz$) of the resonance frequencies with a sampling rate equal to 4 points per wavelength. However, this 12^{th}-order scheme doesn't match the analytical results when the sampling rate is greater than 10 points per wavelength. In the following of this article, all the numerical results are relative the 12^{th}-order finite difference scheme provided in the appendix A.

6 Numerical solution of the coupled problem

Returning to the complete problem, this paragraph presents a numerical solution of the system (16) governing the vibro-acoustic response of a plate coupled with both an infinite fluid domain and a fluid cavity. The plate equations $(16.a, b)$ are discretized with the 12^{th}-order finite difference scheme provided in the appendix A. The acoustic coupling with the exterior domain is ensured by the boundary element method proposed by Mattei in [15]. The equations $(16.f, g, h)$ governing the acoustic pressure inside the cavity are computed in two different ways. The first method is the boundary element method presented in [9]. The second one is a finite difference method based on the second-order central differencing scheme for the second derivative operator presented in the appendix A.

The Green's kernel of the Helmholtz equation in the half-space Ω_e which satisfy the homogeneous Neumann boundary condition on the plane of the plate and the Sommerfeld radiation condition is:
$G(x, z|x', 0) =$

$$\lim_{z'\to 0}\left[-\frac{\imath}{4}H_0\left(k_e\sqrt{(x-x')^2+(z-z')^2}\right)-\frac{\imath}{4}H_0\left(k_e\sqrt{(x-x')^2+(z+z')^2}\right)\right] \quad (20)$$

Using the Green's kernel (20), the solution P_e of the system (16) is written in an integral form:

$$P_e(x,z,k_x,\omega) = -\frac{\imath\omega^2\rho_e}{2}\int_0^L H_0\left(k_e\sqrt{(x-x')^2+z^2}\right)U(x',k_x,\omega)\;dx' \quad (21)$$

Because the Hankel function is singular at the origin, the single layer potential (21) is singular when calculating the function P_e on the plate. This singularity is treated by performing an analytical calculation of the integral (21) on the small interval $[x-\epsilon, x+\epsilon]$ where the single layer potential is singular. The limit of this integral when ϵ tends to zeros is:

$$\int_{x-\epsilon}^{x+\epsilon} H_0(k_e|x-x'|)U(x',k_x,\omega)\;dx' = \epsilon\frac{4\imath}{\pi}\left(\ln(k_e\epsilon)-1\right) \quad 0<\epsilon\ll 1 \quad (22)$$

The Green's representation of the function P_i is written by using the Green's

kernel (20):

$$\begin{aligned} P_i(x,z,k_x,\omega) &= -\frac{\imath\omega^2\rho_i}{2}\int_0^L H_0\left(k_i\sqrt{(x-x')^2+z^2}\right)U(x',k_x,\omega)\,dx' \\ &\quad +\frac{\imath}{2}\int_\sigma H_0\left(k_i r_{M,M'}\right)\alpha(M')\,d\sigma_{M'} \end{aligned} \tag{23}$$

where $r_{M,M'}$ denotes the distance between the point $M(x,z)$ inside the cavity and the point $M'(x',z')$ on the boundary σ of the cavity, and where $\alpha(M)$ $(M \in \sigma)$ is the (unknown) density of the single layer potential (23). The integral (23) is singular when $z = 0$. The contribution of this singularity to the integral (23) is calculated analyticaly by using the formula (22).

7 Discrete Boundary Element Method for the interior Dirichlet problem

This paragraph presents a solution of the system (16) based on the 12^{th}-order finite difference scheme provided in the appendix A for what concerns the plate equations and the Green's representations $(21, 23)$ for the acoustic pressure fields in the two fluid domains Ω_e and Ω_i. A boundary element method, which takes into account the singularity of the single layer potentials, is used to transform the integral equations $(21, 23)$ into a linear set of algebraic equations. This boundary element method is presented in the appendix C, it is based on the Simpson rules.

The boundary σ of the cavity is meshed with M points with the constant step $\Delta\sigma$. Let us denote by M_j the mesh points of the grid. Solving the equation of the displacement of the coupled plate $(16.a)$ by using a n^{th}-order finite difference scheme amounts to solve a system containing $N - n - 4$ algebraic equations. In order to simplify the expressions, a numerical solution is presented for the case of a second-order finite difference discretization scheme of the plate equation. This scheme leads to a system containing $N - 6$ equations for the displacements U_j at the points x_j $(3 \le j \le N-4)$:

$$\begin{aligned} &\frac{D}{\Delta x^4}\left\{U_{j-2} - 4U_{j-1} + 6U_j - 4U_{j+1} + U_{j+2}\right\} \\ &\quad -\omega^2\left\{\mu + \frac{\imath\rho_e}{2}S_e + \frac{\imath\rho_i}{2}S_i\right\}U_j \\ &\quad -\frac{\imath\omega^2\rho_e}{2}\sum_{n=1}^{N-2} W_n H_0\left(k_e R_{j,n}\right)U_n \\ &\quad -\frac{\imath\omega^2\rho_i}{2}\sum_{n=1}^{N-2} W_n H_0\left(k_i R_{j,n}\right)U_n \\ &\quad -\frac{\imath}{2}\sum_{m=1}^{M} W_m H_0\left(k_i r_{j,m}\right)\alpha_m = -e^{\imath k_x x_j}, \quad 3 \le j \le N-4 \end{aligned} \tag{24}$$

The constants W_m and W_n which appear in the equation (24) are the weights of the Simpson's integrals calculated with M points $(m = 1, .., M)$ and N points $(n = 0, .., N-1)$. The term $r_{j,m}$ denotes the distance between the point $(x_j, 0)$ on the plate and the point M_m on the wall σ of the cavity. The term $R_{j,n}$ denotes a distance

resulting from the numerical calculation of the singular integral (21). If $j \neq n$, $R_{j,n}$ is the distance $|x_j - x_n|$ between two points on the plate, if $j = n$, $R_{j,j} = \Delta x$. The terms S_e and S_i, resulting from the analytical calculation (22), are provided in the appendix C. They represent the contribution of the singularity in the single layer potentials (21) and (23). α_m is the density of single layer potential (23) at the point M_m on the inner side of the cavity. The density α_m is calculated by writing the Dirichlet condition at each mesh point M_m:

$$P_i(M_m, k_x, \omega) = 0, \quad 1 \leq m \leq M \tag{25}$$

The Green's representation (23) of the function P_i is introduced in the boundary condition (25). A numerical calculation of the single layer potential (23) which takes into account the singularity of the Hankel function at the origin is provided in the appendix C. Writing the boundary condition (25) amounts to solve the following set of equations:

$$\begin{aligned} &\frac{\imath\omega^2\rho_i}{2} \sum_{n=1}^{N-2} W_n H_0\left(k_i r_{j,n}\right) U_n \\ &+\frac{\imath}{2} \sum_{m=1}^{M} W_m H_0\left(k_i R_{j,m}\right) \alpha_m + \frac{\imath}{2}\epsilon_j S_j = 0, \quad 1 \leq j \leq M \end{aligned} \tag{26}$$

In formula (26), $r_{j,n}$ is the distance between the point M_j on the wall σ and the point $(x_n, 0)$ on the plate; $R_{j,m}$ is a non-zero distance between two mesh points M_j and M_m on the wall σ: If $j = m$, $R_{j,m} = \Delta\sigma$. The term S_j is the contribution of the singularity to the single layer potential 23. The value of the term S_j is given in the appendix C. The term ϵ_j issues from the fact that the contribution of the singularity at the bounds of the plate is half of its contribution elsewhere: If $j = 1, M$, $\epsilon_j = \dfrac{1}{2}$, if $1 < j < M$, $\epsilon_j = 1$.

The boundary conditions (16.b) for the displacement of the clamped plate is obtained by replacing for each index $j = 1,\ 2,\ N-3,\ N-2$, the first line of the equation (24) by the differencing schemes appearing in the formulas (19).

The numerical solution of the coupled system (16) brings to solve the equations (24), with the boundary conditions (19), and the equations (26). This solution leads to inverse a linear set of $M+N-2$ algebraic equations. The unknowns of this system are $N-2$ values U_n of the function $U(x, k_x, \omega)$ calculated at the mesh points x_n on the plate, and M values α_m of the density $\alpha(M)$ calculated at the mesh points M_m on the wall σ of the cavity. This system is solved by a classical LU method. The solutions U_n give access to a discrete expression of the frequency cross spectrum of the displacement of the plate (11). The solutions U_n and α_m, introduced in the Green's representations (21, 23), give access to the functions P_e and P_i which appear in the definitions (12, 15) of the frequency cross spectrum of the acoustic pressure in the two fluid-domains. The spectrums S_{p_e} and S_{p_i} are calculated in a continuous way with respect to the space variable.

8 Finite Difference Method for the interior Dirichlet problem

This section is dedicated to a numerical solution of the system (16) based on the use of an order 12 finite difference scheme for the plate equations, coupled with a boundary element representation for the exterior acoustic pressure field, and with a second-order finite difference method for the interior Dirichlet problem.

The method proposed in this section implies that the mesh-grids of the plate and of the fluid cavity coincide on the $z = 0$ line. Let us denote Δz the sampling-step of the z-dependency of the acoustic pressure inside the cavity. The coordinates of the interior acoustic mesh point $M_{i,j}$ are $(i\Delta x, -j\Delta z)$ with $0 \leq i \leq N-1$ and $0 \leq j \leq M-1$. Because the x meshings of the plate and of the interior acoustic pressure field coincid, when the wavelength of the interior acoustic pressure field is greater than the elastic wavelength (*ie* at high frequency), this method performs an oversampling of the structure. According the results of the Table 1, when this oversampling ecceds 10 points per elastic wavelength, a lower-order finite difference method must be used to solve the plate equation. The results presented in this article are relative to the case of an elastic wavelength greater than the acoustic wavelength. This case is representative of the majority of the practical problems at low frequency.

In order to simplify the expressions, the numerical solution is presented for the case of a second-order differencing scheme for the fourth-order plate operator. The numerical solution of the equation (16.a) leads to the following $N-6$ equations for the displacement of the fluid-loaded plate (apart from the boundary conditions):

$$\begin{aligned} &\frac{D}{\Delta x^4}\left\{U_{j-2} - 4U_{j-1} + 6U_j - 4U_{j+1} + U_{j+2}\right\} \\ &\quad - \omega^2\left\{\mu + \frac{\imath\rho_e}{2}S_e\right\}U_j - P_{j,0} \\ &\quad - \frac{\imath\omega^2\rho_e}{2}\sum_{n=1}^{N-2} W_n H_0\left(k_e R_{j,n}\right)U_n = -e^{\imath k_x x_j}, \quad 3 \leq j \leq N-4 \end{aligned} \tag{27}$$

The boundary conditions for a clamped plate are given by four equations for the displacements of the points x_j, $j = 1$, 2, $N-3$, $N-2$. These equations are obtained by replacing, for each index j, the finite difference scheme appearing in the first line of the formula (27) by the differencing schemes written at the bounds of the plate in the formula (19). The term:

$$-\frac{\imath\omega^2\rho_e}{2}\left\{\sum_{n=1}^{N-2} W_n H_0\left(k_e R_{j,n}\right)U_n + S_e U_j\right\} \tag{28}$$

appearing the the system (27) ensures the exterior acoustic coupling. It results from the numerical evaluation, presented in the appendix C, of the integral (21).

The acoustic coupling with the fluid cavity is ensured by the term $P_{j,0} = P_i(M_{j,0})$ which represents the interior acoustic pressure field, calculated on the plate, at the point $M_{j,0}$ of coordinates $(x_j, 0)$. The interior acoustic pressure field P is the solution of a system composed of the equations (16.f, g, h). The Helmholtz equation (16.f) is

solved by using the second-order central finite difference scheme presented in appendix C. The discretized form of the Helmholtz equation $(16.f)$ is:

$$\begin{aligned} \frac{P_{n-1,m} - 2P_{n,m} + P_{n+1,m}}{\Delta x^2} + \frac{P_{n,m-1} - 2P_{n,m} + P_{n,m+1}}{\Delta z^2} + k_i P_{n,m} = 0 \\ 2 \leq n \leq N-3, \quad 1 \leq m \leq M-3 \end{aligned} \tag{29}$$

The second-order finite difference writing of the Dirichlet boundary condition on the $x = 0$ and $x = L$ walls of the cavity is given by writing the equation (29) for the indexes $n = 0,\ 1,\ N-2,\ N-1$ with the following conditions:

$$\begin{array}{rcccl} n = 0 & : & P_{-1,m} & = & -P_{1,m} \\ n = 1 & : & P_{0,m} & = & 0 \\ n = N-2 & : & P_{N-1,m} & = & 0 \\ n = N-1 & : & P_{N-2,m} & = & -P_{N,m} \end{array} \tag{30}$$

The boundary conditions in the bottom of the cavity results from the writing the equation (29), for the indexes $m = M-2,\ M-1$, with the following conditions:

$$\begin{array}{rcccl} m = M-2 & : & P_{n,M-1} & = & 0 \\ m = M-1 & : & P_{n,M} & = & -P_{n,M-2} \end{array} \tag{31}$$

The boundary conditions at the bottom corners of the cavity are obtained by rewriting the equations (29) for each couple of indexes (m, n) satisfying $m \in \{M-2, M-1\}$ and $n \in \{0, 1, N-2, N-1\}$ with the conditions (30) and (31).

The interior acoustic coupling equation $(16.g)$ is discretized with the second-order central finite difference scheme for the operator $\dfrac{\partial}{\partial x}$ provided in the appendix A:

$$\frac{P_{n,1} - P_{n,-1}}{2\Delta z^2} = \rho_i \omega^2 U_n, \quad 0 \leq n \leq N-1 \tag{32}$$

The boundary condition (32), introduced in the Helmholtz equation (29), leads to a set of $N-4$ equations for the coupling between the vibrations of the plate and the interior acoustic pressure field:

$$\frac{P_{n-1,0} - 2P_{n,0} + P_{n+1,0}}{\Delta x^2} + \frac{2P_{n,1} - 2P_{n,0}}{\Delta z^2} - 2\frac{\rho_i \omega^2}{\Delta z} U_n + k_i P_{n,0} = 0, \quad 2 \leq n \leq N-3 \tag{33}$$

Four equations must be added for the interior acoustic coupling at the bounds of the plate. These equations are obtained by introducing the boundary conditions (30) in the Helmholtz equation (33) written for the indexes $n = 0, 1, N-2, N-1$.

The finite difference method transforms the system of differential equations (16) into a set of $N(M+1)-2$ algebraic equations containing the plate equations (27) with the boundary conditions (19), the discrete Helmholtz equations (29) and (33) with the Dirichlet boundary conditions (30) and (31). The unknowns of this system are the $N-2$ displacements U_n of the points x_n $(1 \leq n \leq N-2)$ and the MN acoustic pressures at the points $M_{n,m}$ $(0 \leq n \leq N-1,\ 0 \leq m \leq M-1)$ inside the cavity. This system is solved by a classical LU algorithm. The solution gives access to a discrete evaluation the function $U(x, k_x, \omega)$, appearing in the definition (11) of the frequency cross spectrum of the displacement, and of the function $P_i(M, k_x, \omega)$ appearing in

the expression (15) of the frequency cross spectrum of the interior acoustic pressure field. The frequency cross spectrums S_u and S_{p_i} are thus evaluated in a discrete way with respect to the space variables. The frequency cross spectrum (12) of the exterior acoustic pressure field is calculated by the same method presented in the precedent paragraph. It results from a numerical evaluation of the integral (21). The function S_{p_e} is then calculated in a continuous way with respect to the space variables.

9 Turbulent boundary layer excitation of a plane panel

The literature provides a large amount of models for the wall pressure fluctuations in a turbulent boundary layer developed over a plane smooth surface. One of the first model is the Corcos spectrum [3]. Corcos developed an empirical model in which the cross-correlation function of the wall pressure fluctuations is approximated by an exponential behaviour. The Corcos wavenumber-frequency power spectrum expresses as follow:

$$S(k_x, k_y, \omega) = \Phi_0(\omega) \left[\alpha\beta \left(\omega/u_c\right)^2\right] / \left\{\pi^2 \left[\left(k_x - \omega/u_c\right)^2 + \left(\alpha\omega/u_c\right)^2\right] \left[k_y^2 + \left(\beta\omega/u_c\right)^2\right]\right\} \tag{34}$$

where k_x and k_y are the wavenumbers in the directions parallel to the x-axis and y-axis. A broad band model of the point power spectrum $\Phi_0(\omega)$ is:

$$\Phi_0(\omega) = a_+ \left(1 + \gamma\right) \rho_e \nu_*^4 / \omega \tag{35}$$

Let us remaind that more sofisticated larger band expressions for the point power spectrum $\Phi_0(\omega)$ are provided in the literature [10]. The value of the constants in this Corcos model are $\alpha = 0.09$, $\beta = 7\alpha$, $a_+ = 0.766$ and $\gamma = 0.389$. The convective velocity u_c is taken equal to $0.7u_\infty$, where u_∞ is the speed of the fluid flow. The friction velocity is simply given equal to $\nu_* = 0.03u_\infty$.

In 1980 Chase [11] proposed a more rigorous model for an incompressible fluid which include higher subconvective wavenumbers. In 1987 Chase [4] reformulated this model in order to include the effects of the compressibility. The Chase wavenumber-frequency power spectrum is given as follows:

$$S(k_x, k_y, \omega) = S_m(k_x, k_y, \omega) + S_t(k_x, k_y, \omega) \tag{36}$$

where S_m represents the contribution of the mean shear to the wall pressure fluctuations spectrum:

$$S_m(k_x, k_y, \omega) = \frac{C_M \rho_e^2 \nu_*^3 k_x^2}{\left[\left(\omega - k_x u_c\right)^2 / \left(h_m \nu_*\right)^2 + k^2 + 1/\left(b_m \delta\right)^2\right]^{(5/2)}}$$

and where S_t concerns the contribution of the pure turbulence to the wall pressure fluctuations spectrum:

$$S_t(k_x, k_y, \omega) = \frac{C_T \rho_e^2 \nu_*^3 k^2}{\left[\left(\omega - k_x u_c\right)^2 / \left(h_t \nu_*\right)^2 + k^2 + 1/\left(b_t \delta\right)^2\right]^{(5/2)}}$$

The parameters of the Chase model are the thickness δ of the boundary layer and the following constants: $k^2 = k_x^2 + k_y^2$, $C_T = 3r_t a_+ / 2\pi h_t$, $C_M = (c_t + r_m)/r_t$, $h_m =$

$\mu_m u_c/\nu_*$, $h_t = \mu_t u_c/\nu_*$, $r_t = 0.389$, $r_m = 0.611$, $a_+ = 0.766$, $\mu_m = \mu_t = 0.176$, $b_m = 0.756$, $b_t = 0.378$. The contribution of the subconvective wavenumbers in the Chase model are approximately of $20dB$ lower than those predicted by the Corcos model. For a one-dimensional plate, the wavenumber-frequency cross spectrum of the wall pressure fluctuations in the direction parallel to the flow are given by the two-dimensional models (34) and (36) in which the transvers wavenumber k_y is taken equal to zero.

10 Numerical results

This section proposes two studies based on the numerical results obtained on a representative test case: In a two-dimensional space, we consider a one-dimensional plate coupled on one side with an infinite fluid domain and on the other side with a fluid cavity. The numerical results consist in the power spectrums of the displacement of the plate and of the acoustic pressure fields in Ω_e and Ω_i given by the formulas $(11, 12, 15)$ where $x = y$ and $M = M'$. These spectrums are calculated by solving the coupled system of differential equation (16). The first study concerns the influence of the method used to solve the interior acoustic problem. The second study focuses on the influence of the model of turbulence on the vibro-acoustic response of the physical system. The data for this test case are presented bellow:

1. Plate Σ:
   - Boundary conditions: Clamped
   - Length $L = 1m$ (air) and $L = 0.5m$ (water)
   - Thickness $e = 0.004m$ (air) and $e = 0.005m$ (water)
   - Young modulus $E = 2\,10^{11} Nm$
   - Poisson ratio $\nu = 0.3$
   - Mass per unit area $\mu = 7800 \cdot e\ Kgm^{-2}$
   - Mesh-grid $N = 60$ points
2. Fluid cavity Ω_i:
   - Boundary conditions: Dirichlet
   - Height $H = 0.5m$
   - Mesh-grid $N \times M = 60 \times 30$ points
3. Exterior fluid domain Ω_e: Flow velocity $u_\infty = 10m/s$
4. Water
   - Mass per unit volume $\rho_{e/i} = 1000\ Kgm^{-3}$
   - Sound velocity $c_{e/i} = 1460m/s$
5. Air
   - Mass per unit volume $\rho_{e/i} = 1.23\ Kgm^{-3}$
   - Sound velocity $c_{e/i} = 340m/s$

6. Measurement points

   - Displacement: $x = L/4$
   - Interior acoustic pressure: M_i = middle of the cavity
   - Exterior acoustic pressure: M_e = symetric of M_i with respect the plate

10.1 Comparison of the finite difference / boundary element solutions of the interior Dirichlet problem

The numerical results presented in this section concern the Corcos spectrum (34) and an acoustic coupling with air in ω_e and Ω_i. The results obtained with three numerical methods are compared.

- **FD-BEM**: An order 12 finite difference method is performed to solve the plate equations and coupled with a boundary element method for solving the interior Dirichlet problem (see section 7).
- **FD-FD**: Two coupled finite difference methods of respective orders 12 and 2 for the displacement of the plate and for the interior acoustic pressure fields (see section 8).
- **BEM-BEM**: We compare these curves with the results coming from the code NOVALEA2D developed at the Laboratoire de Mécanique et d'Acoustique de Marseille. NOVALEA2D uses a boundary element representation for both the displacement of the plate and the acoustic pressure fields.

We must note that, in order to obtain a good accuracy with this NOVALEA2D code, we need to use a sampling rate of 12 points per elastic wavelength.

The figure 1 presents the power spectrum of the acceleration of the plate at the point x = L/4. The figure 2 provides the power spectrum of the acoustic pressure in the exterior domain. Note that due to the symmetry, only the odd beam modes generate high acoustic levels at this particular calculation point. The figures 1 and 2 present a good agreement between the 3 numerical methods. The figure 3 presents the power spectrum of the acoustic pressure inside the cavity. On this last figure, a difference appears between the results obtained with the finite difference and the boundary element representations of the cavity. With the finite difference method (FD-FD), we observe an acute peak located at the first resonance frequency of the cavity. Because of the *light*-fluid coupling, this first resonance frequency is very close to the first resonance frequency of a rigid cavity involving 3 Dirichlet conditions and a Neumann condition in place of the plate. With the boundary element representations of the interior acoustic pressure field (FD-BEM and BEM-BEM), no strong excitation is evident around this cavity mode.

10.2 Influence of model of turbulence

The results presented in this section concern an acoustic coupling with water. We focus on the differences arising when the turbulent wall pressure fluctuations are modeled by the Corcos spectrum (34) and by the Chase spectrum (36). These Corcos and Chase models are presented at the frequency $2000Hz$ on the figure 4. In the subconvective region (*ie* for $k_x/k_e < 100$) these models differ by $20dB$. The figure

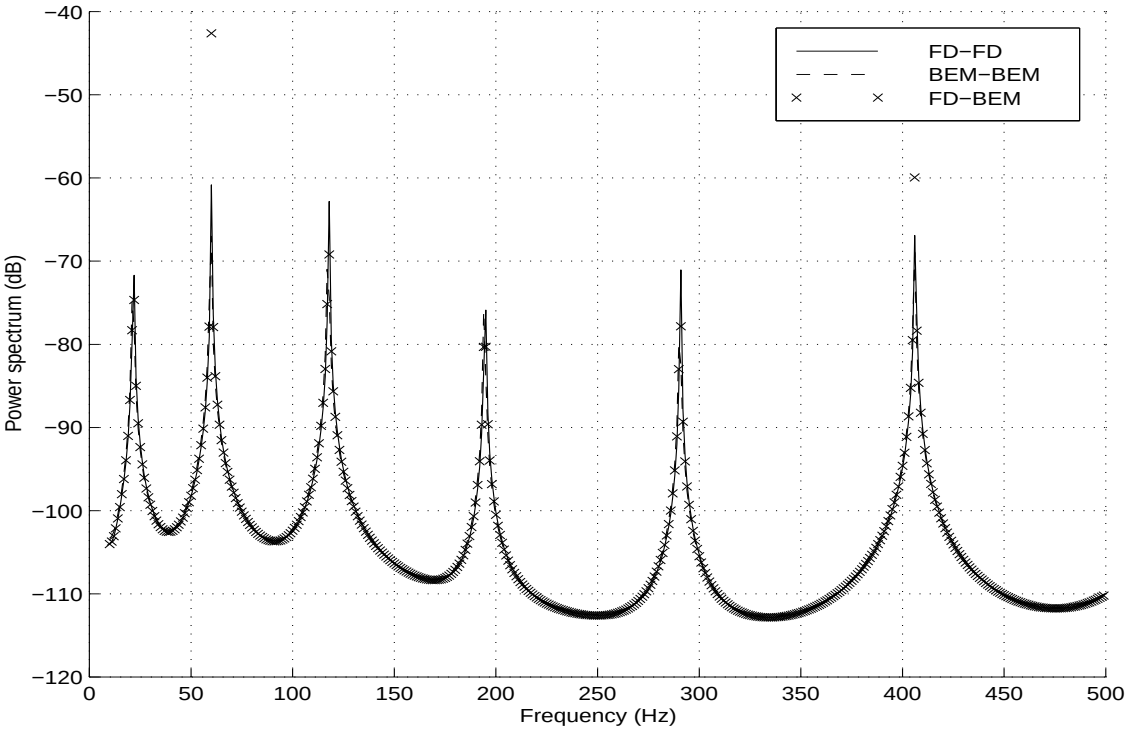


Figure 1: Acceleration of the plate at the point x = L/4 (air)

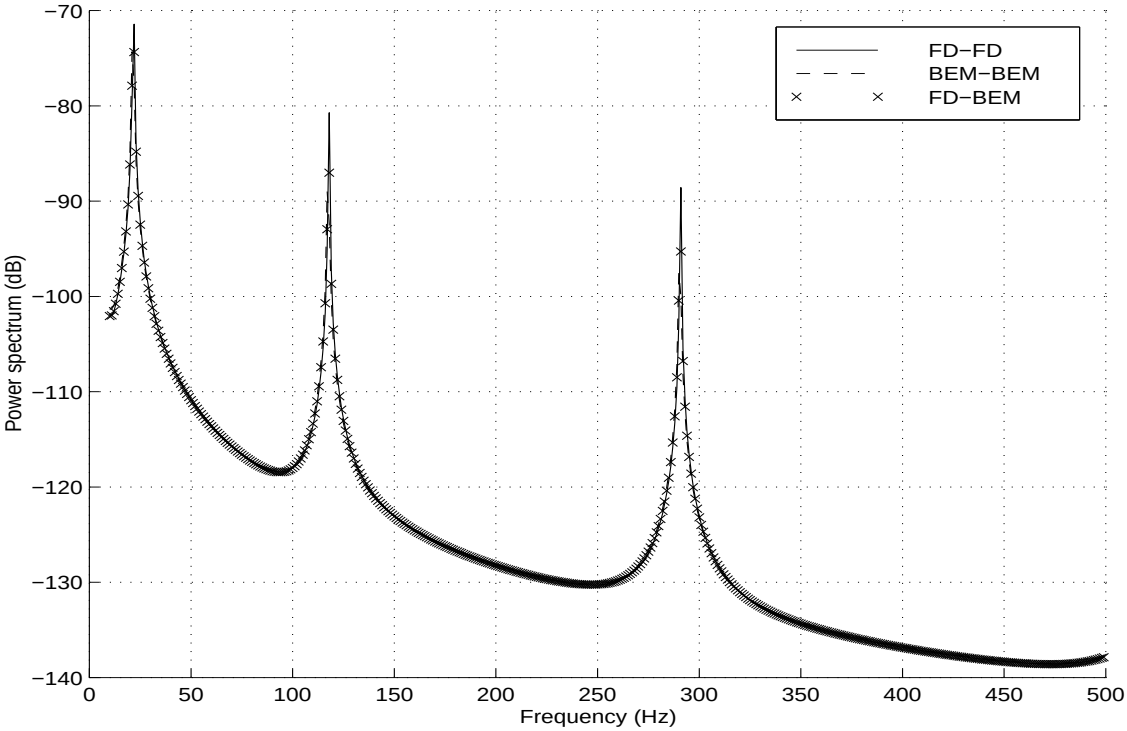


Figure 2: Acoustic pressure in the exterior domain (air)

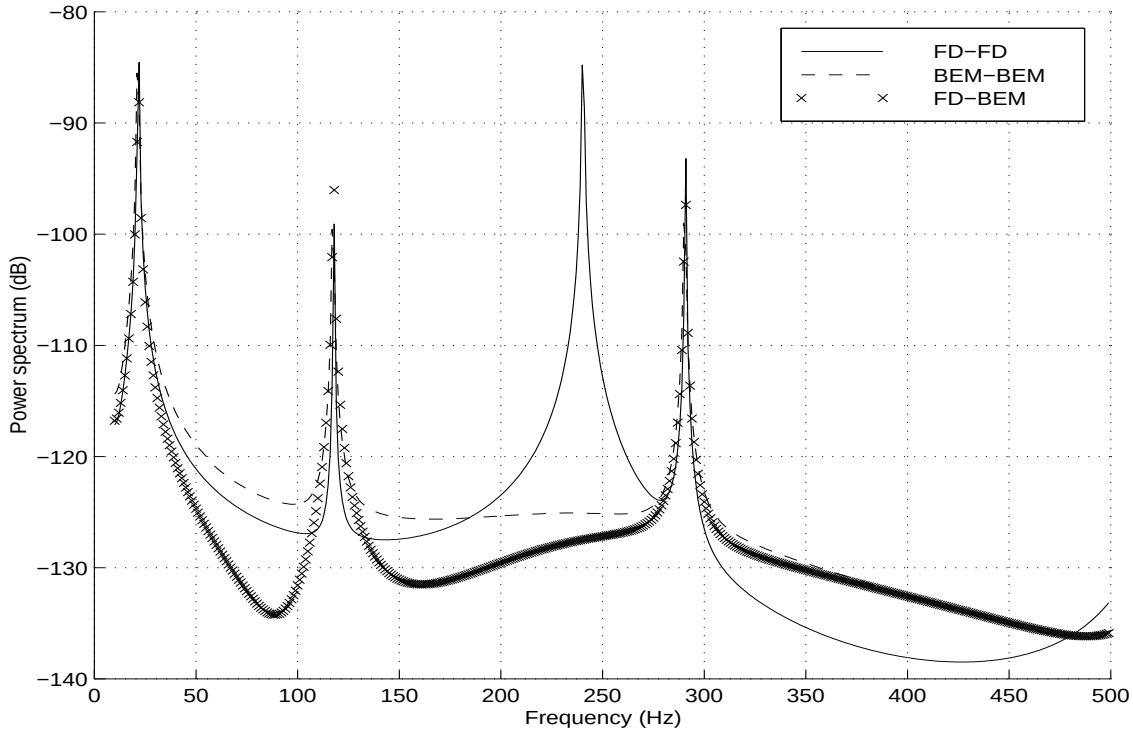


Figure 3: Acoustic pressure inside the cavity (air)

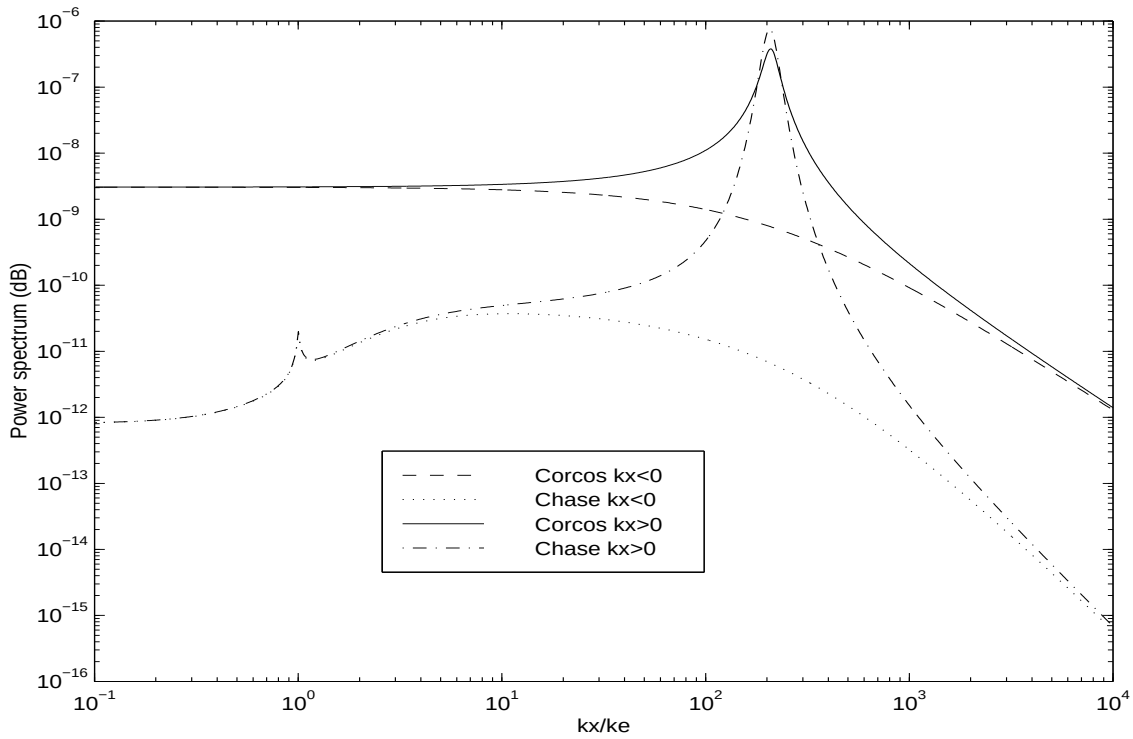


Figure 4: Models of turbulence (water)

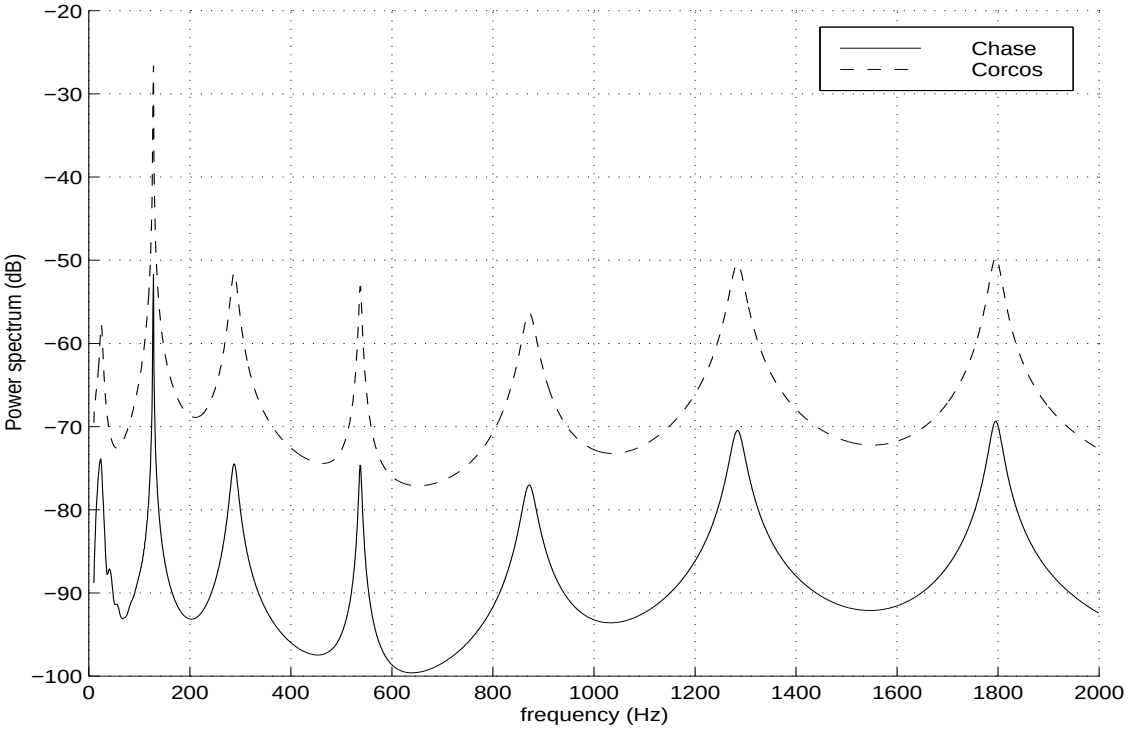


Figure 5: Acceleration of the plate (water)

5 shows the power spectrum of the acceleration of the plate. The figure 6 concerns the interior acoustic pressure field. These two figures present the same behaviour: The results obtained with the Chase model are $20dB$ under the predictions obtained with the Corcos model. The results presented on figures 5 and 6 confirm the results presented in [16] and calculated with the NOVALEA2D code. A study of this difference is presented in [5]: Because The transfer function of the displacement of the plate (14) presents an important peak located at the origin ($k_x = 0$), the intantaneous spectral density function (13) is maximum in the region of the subconvective wavenumbers. So, the influence of the flow on the vibro-acoustic responses (11) (12) and (15) arise mainly from the behaviour of the wall pressure fluctuations spectrum S_f in the subconvective region. So, because the Corcos and Chase models differ by approximately $20dB$ in the subconvective domain, the vibro-acoustic responses of our physical system also differ by $20dB$.

11 Conclusion

This paper presents a simple model for the vibro-acoustic responses of a plane panel excited by a turbulent boundary layer. This model applies provided the wall pressure fluctuations are given under the form of a wavenumber-frequency power spectrum. The first interest of this model is that the ($\mathbf{k}$-ϵ) formalism permits to take into account the most recent advances in the modeling of turbulence. The second interest lies in the greater computational performances of the wavenumber-domain integral (11) on the space-domain double integral (9).
Our second aim in this article is to study the numerical efficiency of an high-order finite difference method applied to the resolution of a plate equation. The Table 1

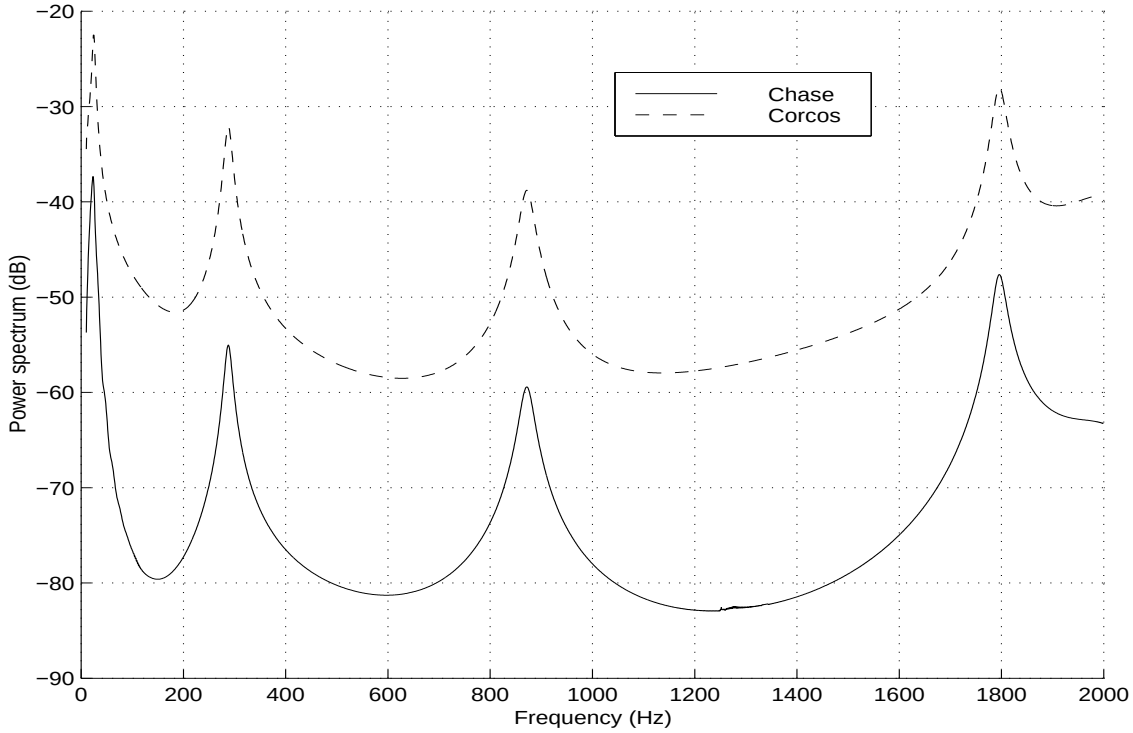


Figure 6: Acoustic pressure inside the cavity (water)

and the figures 1, 2 and 3 show that an order 12 finite difference scheme is a very efficient tool to solve a plate equation, particilarly adapted to small sampling rates between 4 and 10 points per wavelength.
Concerning the advantages and the inconvenients inherent to the use of a boundary element method or of a finite difference method to solve an interior acoustic problem, the figure 3 shows that the difference concerns the behaviour of the physical system at the resonance of the cavity : The finite difference method calculates a strong peak whereas the boundary element method shows a very smooth peak. However, it is not possible to discuss the validity of one of these two methods with the results presented in this article. An experiment is necessary. Discussing the advantages and disadvantages of the boundary element versus the finite difference approaches, we can point out that the finite difference method can be quite memory consuming when applied to large scale problems. On the other hand, the finite difference method is perhaps more flexible. Local boundary conditions, irregular cavity shapes, and non-constant beam parameters might be included.

APPENDIX A
Central finite difference schemes

This appendix presents the expressions of central the central finite difference schemes for following the derivative operators: $\dfrac{\partial}{\partial x}$ which appears in the discretization of the coupling equation, $\dfrac{\partial^2}{\partial x^2}$ used for the calculation of the Helmholtz equation and $\dfrac{\partial^4}{\partial x^4}$ appearing in the plate equation.
Order 2 finite difference scheme for the first derivative

$$\frac{d}{dx}f = \frac{f(x+h) - f(x-h)}{2\,h}$$

Order 2 finite difference scheme for the second derivative

$$\frac{d^2}{dx^2}f = \frac{f(x-h) - 2\,f(x) - f(x+h)}{h^2}$$

Order 2 finite difference scheme for the fourth derivative

$$\frac{d^4}{dx^4}f = \frac{f(x-2\,h) - 4\,f(x-h) + 6\,f(x) - 4\,f(x+h) + f(x+2\,h)}{h^4}$$

Order 4 finite difference scheme for the fourth derivative

$$\begin{aligned}\frac{d^4}{dx^4}f \;&= \frac{1}{h^4}\;\left(-\frac{1}{6}\,f(x-3\,h) + 2\,f(x-2\,h) - \frac{13}{2}\,f(x-h) + \frac{28}{3}\,f(x)\right.\\ &\left. -\frac{13}{2}\,f(x+h) + 2\,f(x+2\,h) - \frac{1}{6}\,f(x+3\,h)\right)\end{aligned}$$

Order 6 finite difference scheme for the fourth derivative

$$\begin{aligned}\frac{d^4}{dx^4}f \;&= \frac{1}{h^4}\;\left(\frac{7}{240}\,f(x-4\,h) - \frac{2}{5}\,f(x-3\,h) + \frac{169}{60}\,f(x-2\,h)\right.\\ &\quad - \frac{122}{15}\,f(x-h) + \frac{91}{8}\,f(x) - \frac{122}{15}\,f(x+h)\\ &\left.\quad +\frac{169}{60}\,f(x+2\,h) - \frac{2}{5}\,f(x+3\,h) + \frac{7}{240}\,f(x+4\,h)\right)\end{aligned}$$

Order 12 finite difference scheme for the fourth derivative

$$\begin{aligned}\frac{d^4}{dx^4}f \;&= \frac{1}{h^4}\;\left(-\frac{713664}{46142992981}\,f(x-7\,h) + \frac{22426211628299}{20930461616181600}\,f(x-6\,h)\right.\\ &\quad - \frac{19}{1050}\,f(x-5\,h) + \frac{643}{4200}\,f(x-4\,h) - \frac{4969}{5670}\,f(x-3\,h)\\ &\quad + \frac{4469}{1120}\,f(x-2\,h) - \frac{1769}{175}\,f(x-h)\\ &\quad + \frac{37037}{2700}\,f(x) - \frac{1769}{175}\,f(x+h) + \frac{4469}{1120}\,f(x+2\,h)\\ &\quad - \frac{4969}{5670}\,f(x+3\,h) + \frac{643}{4200}\,f(x+4\,h) - \frac{19}{1050}\,f(x+5\,h)\\ &\left.\quad +\frac{22426211628299}{20930461616181600}\,f(x+6\,h) - \frac{713664}{46142992981}\,f(x+7\,h)\right)\end{aligned}$$

APPENDIX B
Troncation error analysis

In this appendix, we present the calculation of the truncation error made when replacing the differential operator $d^4f(x)/dx^4$ by the following finite difference scheme:

$$\frac{f(x-2\,h) - 4\,f(x-h) + 6\,f(x) - 4\,f(x+h) + f(x+2\,h)}{h^4} \qquad A2.1$$

The truncation error e is given by the difference:

$$e = \frac{f(x-2\,h) - 4\,f(x-h) + 6\,f(x) - 4\,f(x+h) + f(x+2\,h)}{h^4} - \frac{d^4}{dx^4} f(x) \qquad A2.2$$

The functions $f(x-2\,h)$, $f(x-\,h)$, $f(x+\,h)$ and $f(x+2\,h)$ are expressed by the following Taylor series:

$$f(x-2\,h) = f(x) - 2h\frac{df(x)}{dx} + 2h^2\frac{d^2f(x)}{dx^2} - \frac{4h^3}{3}\frac{d^3f(x)}{dx^3}$$

$$+ \frac{2h^4}{3}\frac{d^4f(x)}{dx^4} - \frac{4h^5}{15}\frac{d^5f(x)}{dx^5} + \frac{4h^6}{45}\frac{d^6f}{dx^6}(\alpha)$$

where α is a real number between 0 and h.

$$f(x-\,h) = f(x) - h\frac{df(x)}{dx} + \frac{h^2}{2}\frac{d^2f(x)}{dx^2} - \frac{h^3}{6}\frac{d^3f(x)}{dx^3}$$

$$+ \frac{h^4}{24}\frac{d^4f(x)}{dx^4} - \frac{h^5}{120}\frac{d^5f(x)}{dx^5} + \frac{h^6}{720}\frac{d^6f}{dx^6}(\alpha)$$

$$f(x+\,h) = f(x) + h\frac{df(x)}{dx} + \frac{h^2}{2}\frac{d^2f(x)}{dx^2} + \frac{h^3}{6}\frac{d^3f(x)}{dx^3}$$

$$+ \frac{h^4}{24}\frac{d^4f(x)}{dx^4} + \frac{h^5}{120}\frac{d^5f(x)}{dx^5} + \frac{h^6}{720}\frac{d^6f}{dx^6}(\alpha)$$

$$f(x+2\,h) = f(x) + 2h\frac{df(x)}{dx} + 2h^2\frac{d^2f(x)}{dx^2} + \frac{4h^3}{3}\frac{d^3f(x)}{dx^3}$$

$$+ \frac{2h^4}{3}\frac{d^4f(x)}{dx^4} + \frac{4h^5}{15}\frac{d^5f(x)}{dx^5} + \frac{4h^6}{45}\frac{d^6f}{dx^6}(\alpha)$$

Introducing these Taylor series in the formula $(A2.2)$ leads to the expression of the truncation error:

$$e = \frac{3h^2}{18}\frac{d^6f}{dx^6}(\alpha) \quad \text{with:} \quad 0 \le \alpha \le h$$

So, the order of accuracy of the finite difference scheme $(A2.1)$ is $O(h^2)$.

APPENDIX C
Boundary element method

In this appendix, we present the numerical calculation of the single layer potential (21) appearing in the expression of the exterior acoustic pressure field:

$$\int_0^L H_0\left(k_e\sqrt{(x_j-x)^2+z^2}\right) U(x,k_x,\omega)\; dx \qquad A3.1$$

This integral becomes singular when calculating the acoustic pressure on the plate (ie for z=0). Let us suppose that the singular point x_j is not located at the bounds $\partial\Sigma$ of the plate. The singular integral $(A3.1)$ is calculated by using the Simpson rules:

$$\begin{aligned} \int_0^L H_0\left(k_e\,|x_j-x|\right) U(x,k_x,\omega)\; dx \quad &\sim \quad \sum_{n=1}^{N-2} W_n H_0\left(k_e R_{j,n}\right) U_n \\ -2\,U_j\,\Delta x H_0\left(k_e\Delta x\right) \quad &+ \quad U_j \int_{x_j-\Delta x}^{x_j+\Delta x} H_0\left(k_e\,|x_j-x|\right)\; dx \end{aligned} \qquad A3.2$$

where $R_{j,n} = |x_j - x_n|$ if $j \neq n$ and $R_{j,j} = \Delta x$, and where W_n are the weights of the Simpson integral calculated with N points when the contributions of the first point (index 0) and of the last point (index N-1) to this integral are known to be equal to zero:

$$W_n = \{4, 2, 4, 2, ...4, 2, 4, 2, 4\} \quad \text{N-2 times}$$

The first right-hand term appearing in the formula ($A3.2$):

$$\sum_{n=1}^{N-2} W_n H_0 \left(k_e R_{j,n}\right) U_n \qquad A3.3$$

is a Simpson estimation of the singular integral ($A3.1$) calculated when the value of the Hankel function at the singular point x_j is arbitrary taken equal to its values at the points before and after x_j:

$$H_0(0) \longrightarrow H_0\left(|x_j - x_{j-1}|\right) = H_0\left(|x_j - x_{j+1}|\right) = H_0\left(\Delta x\right)$$

The term $2\,\Delta x\, U_j\, H_0\left(k_e \Delta x\right)$ substracts, in the Simpson integral ($A3.3$), the contribution of the interval $[x_j - \Delta x, x_j + \Delta x]$ containing the singular point x_j. The contribution of the domain $[x_j - \Delta x, x_j + \Delta x]$ is reintroduced in the final result under the following form:

$$U_j \int_{x_j - \Delta x}^{x_j + \Delta x} H_0\left(k_e \left|x_j - x\right|\right)\, dx \qquad A3.4$$

Writting the integral ($A3.4$), we suppose that the function $U(x, k_x, \omega)$ has slow variations on the small domain $[x_j - \Delta x, x_j + \Delta x]$. Performing two changes of variables, $Y = x_j - x$ and $X = k_e Y$, and introducing the behaviour of the Hankel function at the origin:

$$X \sim 0 \longrightarrow H_O(X) \sim \frac{2\,\imath}{\pi} \ln(x)$$

leads to the following approximation for the integral ($A3.4$):

$$\int_{x_j - \Delta x}^{x_j + \Delta x} H_0\left(k_e \left|x_j - x\right|\right)\, dx \sim \frac{2}{k_e} \int_{k_e \epsilon}^{k_e \Delta x} H_O(x)\, dx + \frac{4\imath}{\pi} \epsilon \left(\ln\left(k_e \epsilon\right) - 1\right)$$

Let us denote S_e the term introducing the contribution of the singularity of the Hankel function at the origin when calculating the integral $A3.1$ over the plate domain:

$$S_e = \frac{2}{k_e} \int_{k_e \epsilon}^{k_e \Delta x} H_O(x)\, dx + \frac{4\imath}{\pi} \epsilon \left(\ln\left(k_e \epsilon\right) - 1\right) - 2\,\Delta x H_0\left(k_e \Delta x\right)$$

The definition of S_e contains an integral on the small interval $[k_e \epsilon, k_e \Delta x]$. This integral is calculated numericaly by the classical Simpson rules. This expression of S_e gives access to an approximation of the singular integral ($A3.1$) calculated on the plate:

$$\int_0^L H_0\left(k_e \sqrt{(x_j - x)^2}\right) U(x, k_x, \omega)\, dx \sim S_e\, U_j + \sum_{n=1}^{N-2} W_n H_0\left(k_e R_{j,n}\right) U_n$$

References

[1] J.H. Ducan, J.S. Sirkis 1992 *Journal of Sound and Vibration* **15**(2), 243-264. The generation of wave patterns on anisotropic coatings by pressure fluctuations in a turbulent boundary layer.

[2] M.S. Howe 1992 *Journal of the Acoustical Society of America* **91**(1), 91-98. The wall-pressure spectrum in turbulent flow over a randomly inhomogeneous elastic solid.

[3] G.M. Corcos 1963 *Journal of the Acoustical Society of America* **35**(2), 192-199. Resolution of presure in turbulence.

[4] D.M. Chase 1987 *Journal of Sound and Vibration* **112**, 125-147. The character of the turbulent wall pressure spectrum at subconvective wavenumbers and a suggested comprehensive model.

[5] D. Mazzoni 1994 *Sur le rayonnement acoustique de sources aléatoires : problème direct et problème inverse (réf. 2079448).* Thèse, Université d'Aix-Marseille II, Institut de Mécanique de Marseille, UNIMECA, Institut Méditerrannéen de Technologie, Chemin de la Grave, 13451 MARSEILLE CEDEX 20, FRANCE.

[6] U. Kristiansen 1997 Paper submitted to the *Journal of Sound and Vibration.* A finite difference scheme for the coupled plate/cavity problem - a 2D example.

[7] Huw G. Davies 1971 *Journal of the Acoustical Society of America* **49**(3, part 2) 878-889. Sound from turbulent-boundary-layer-excited panels.

[8] G. Robert 1984 *Modélisation et simulation du champ excitateur induit sur une structure par une couche limite turbulent (réf. E.C.L. 84-02).* Thèse, Ecole Centrale de Lyon, 36 avenue Guy Collongue, B.p. 163, 69131 ECULLY, FRANCE.

[9] P. Filippi, D. Mazzoni Noise inside a cavity due to an external turbulent boundary layer. BEM16, 13-15 july 1994, Southampton, England.

[10] S. Bano, R. Marney, L. Jourdan and J.-P. Guibergia 1992 *Journal d'Acoustique* **5**, 99-124. Etude théorique et expérimentale de la réponse vibro-acoustique d'une plaque couplée â une cavité en fluide lourd.

[11] D.M. Chase 1980 *Journal of Sound and Vibration* **70**, 29-67. Modeling the wavevector-frequency spectrum of turbulent boundary layer wall pressure.

[12] D.M. Chase 1990 *Journal of the Acoustical Society of America* **90**(2), 1032-1040. The wave-vector-frequency spectrum of pressure on a smooth plane in turbulent boundary layer flow at low Mach number.

[13] P. Krée, C. Soize 1983 *Mécanique aléatoire.* Dunod - Bordas, Paris.

[14] A. Leissa 1993 *Vibration of plates.* Acoustical Society of America. Originally issued by NASA, 1973.

[15] P.-O. Mattei 1995 *Journal of Sound and Vibration* **179**(1), 63-77. Sound radiation by baffled and constrained plates.

[16] P. Filippi, D. Mazzoni 1997 *Uncertainty Modeling in Finite Element, Fatigue and Stability of Structures (Series on Stability, Vibrations and Control of Systems* vol. **9**, 117-158. Response of a vibrating structure to a turbulent wall pressure : fluid-loaded structure modes series and boundary element method. WorldScientific.